Underwater ERT surveying in water with resistivity layering with example of application to site investigation for a rock tunnel in central Stockholm

Dahlin, Torleif; Loke, Meng Heng

Published in:
Near Surface Geophysics

DOI:
10.3997/1873-0604.2018007

2018

Document Version:
Publisher's PDF, also known as Version of record

Near Surface Geophysics, 2018, **16**, 230-237 doi:10.3997/1873-0604.2018007

Underwater ERT surveying in water with resistivity layering with example of application to site investigation for a rock tunnel in central Stockholm

Torleif Dahlin[1*], Meng Heng Loke[2]

[1] *Engineering Geology, Lund University, Box 118, SE-22100 Lund, Sweden*
[2] *Geotomo Software, 115 Cangkat Minden Jalan 6, 11700 Gelugor, Penang, Malaysia*

Received September 2017, revision accepted March 2018

ABSTRACT

We present an approach to underwater electrical resistivity tomography surveying under conditions with several water layers with different resistivity in the water above the electrode layout. The approach is verified against a synthetic model example and tested in full scale on data from a field survey. The field survey was carried out in central Stockholm as part of pre-investigations for a new metro train (T-bana) tunnel planned to pass under seawater. The water passage is associated with major tectonic zones that can potentially be very difficult from a tunnel construction point of view. The aim was to identify variations in depth of the bottom sediments and variations in rock quality including the possible presence of weak zones in the rock. Survey conditions are complicated by boat traffic and electrical disturbances from the power grid and train traffic. The water depth was mapped using sonar combined with recording pressure transducers, and water resistivity as a function of water depth was recorded using geophysical borehole logging equipment. Water resistivity as a function of depth was integrated in the inversion model. The results show that the rather difficult survey conditions could be handled in a satisfactory way thanks to adequate equipment, careful planning, and attention to details. The measured data contain information that is relevant for creating coherent models of the variation in depth to rock, which corresponds well with data from drilling. The results also indicate that information in variation in rock quality that can be of critical importance for planning of underground construction can be derived from the data.

Key words: ERT, Resistivity, Underwater, Tunnel, Pre-investigation.

INTRODUCTION

There is a need of information regarding depth to bedrock and weak zones in the rock for underground construction purposes, since unforeseen weak and water bearing zones, as well as insufficient rock cover, can lead to severe delays and cost increases in the construction phase. In Stockholm, several tunnels are planned for various purposes, including tunnels for underground metro trains, roads, sewage, and high tension power supply. For all these purposes, the planned tunnels will include one or more underwater passages. The underwater passages are expected to pose large risks to the construction works, including risk for highly permeable or unstable zones in the rock and insufficient rock cover above the tunnel. The water passages are sections with high risk, as the location of the water passages is not a coincidence but is coupled to the weakest part of the rock mass. Furthermore, pre-investigation with methods such as drilling and mechanical sounding can be subject to limitations because of cables on the sea bottom for which the location is not well documented, thus leading to restrictions. The existence of cables on the bottom limits the applicability of electromagnetic methods, and seismic surveying may be hampered by gas in bottom sediments. Electrical resistivity tomography (ERT) has a potential to function well under such conditions and has been tested in the work presented here.

ERT has been applied to tunnel pre-investigation on land for a couple of decades and proved to provide very relevant and useful results relating to variation rock quality and depth to bedrock (Dahlin, Bjelm and Svensson 1999; Ganerød *et al.* 2006; Danielsen and Dahlin 2009; Rønning *et al*. 2013). Tunnel-to-surface ERT (Simyrdanis et al. 2015b) is a possible follow-up method that could be used for example for characterising the rock mass above a tunnel in more detail than is possible from surface ERT alone, where the results might serve as an aid for planning additional grouting or design of reinforcement.

* Torleif.Dahlin@tg.lth.se

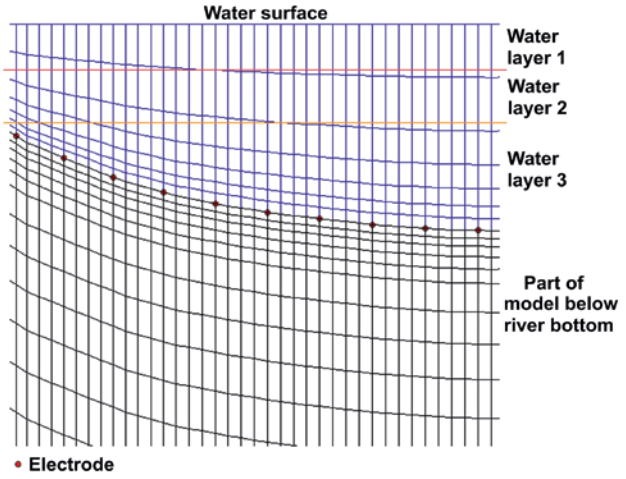

Figure 1 Schematic diagram of part of the finite-element mesh used to model the water layer and sub-bottom materials. The part of the mesh used to model the water layer is drawn in blue.

Underwater resistivity surveying has been tested before with different objectives. Lile *et al*. (1994) successfully detected fracture zones underneath sediments on the sea bottom using a pole–dipole array, as pre-investigation for a tunnel. They concluded that the sediment thickness was difficult to resolve, but it should be noted that the data density and inversion techniques were not comparable with what we use today. Tassis *et al*. (2014) carried out synthetic modelling to assess the resolution of ERT for fracture zone detection in marine environments and concluded that the results can be promising under certain conditions but at the same time be ambiguous since they suffer from reduced resolution and major artificial effects due to short circuiting in the conductive sea water. Ronczka *et al*. (2017) combined ERT with seismic refraction tomography across a passage with brackish water. Their results showed that both methods were consistent in detecting a previously unknown several tens of metres deep zone with low resistivity and low velocity, interpreted as a sediment-filled valley. ERT also indicated the presence of a major fracture zone that had earlier been mapped in a tunnel underneath, although with an unexpected dip. Tsourlos and Tsokas (2004) successfully used underwater ERT for surveying and quantifying potentially polluted sediments in waterways. Orlando (2013) studied the performance and limits of ERT for detection and characterisation of thin near-bottom sedimentary layers, where the analysis included the resolution of floating and submerged electrode cables. The effectiveness of ERT as a tool for assessing groundwater or surface water interactions within streams was investigated by Nyquist, Freyer and Toran (2008), who concluded that patterns of ground water discharge can be mapped at a detailed scale. Nyquist, Heaney and Toran (2009) concluded that towed resistivity is useful as a rapid reconnaissance tool for mapping geologic heterogeneity. The results can be used to position more time-consuming but higher-resolution lake-bottom resistivity measurements, which in turn can guide the placement of *in situ* investigations such as seepage metering. Sea-bottom archaeological investigation is another application for which underwater ERT has been applied successfully (Simyrdanis et al. 2015a).

In all previous works, to our knowledge, the water layer above a bottom electrode layout has been assumed to be homogeneous. We present an approach in which we take into account several water layers with different resistivity in the water body above the bottom electrode cable layout. The theoretical foundation is presented briefly along with a synthetic and a field example with data acquired in layered fresh and brackish water in an urban area.

NUMERICAL MODELLING AND DATA INVERSION

The inversion of apparent resistivity data to obtain a numerical model for the subsurface is inherently non-unique. Available information about the subsurface structure and resistivity distribution should be incorporated into the inversion process to reduce the ambiguity in the data inversion. The known information from the survey is the topography of the sea, lake, or river bottom and the resistivity of the water layers above it, for simplicity referred to as sea bottom in the following. As the water layer typically has a lower resistivity than the materials below the river bed, a large proportion of the electric current flows through the water. Thus, it is important that the effect of the water layer is accurately modelled. A finite-element mesh (Silvester and Ferrari 1990) is used to model the water layer and the subsurface below the sea (Figure 1). The mesh uses four horizontal nodes between adjacent electrode positions that provide a reasonable compromise between ensuring sufficient accuracy and minimizing the calculation time (Dey and Morrison 1979). The part of the finite-element mesh used to model the water layer has 8 to 16 nodes in the vertical direction, as shown by the blue part of the mesh in Figure 1. The number of vertical nodes is adjusted depending on the ratio of maximum thickness of the water layer to the spacing between the electrodes. The vertical distances between the nodes are scaled to fit the thickness of water column above each electrode. A smaller vertical node spacing (of not more than one quarter of the electrode spacing) is used at the bottom of the water mesh, as the electric potential values vary more rapidly near the electrodes. The vertical node spacing is then progressively increased towards the water surface. There is a significant variation of the water resistivity with depth in the survey area (Figure 1). To model the change of water resistivity with depth with sufficient accuracy, the water layer is divided into up to five layers with different resistivities in the inversion of the field data. The resistivity of a finite-element cell is set to the water layer resistivity where it is located. Cells that straddle two layers are assigned a weighted average of the resistivities of the two layers. The lower part of the finite-element mesh (shown in black in Figure 1) is used to model the region below the sea bottom. The resistivity of the finite-element mesh in the water layer is kept fixed during the data inversion process. The sub-

bottom region is subdivided into a number of model cells as in a normal 2D inversion problem (Loke and Barker 1996). The smoothness-constrained least-squares optimisation method is for data inversion (Loke, Acworth and Dahlin 2003). The linearised least-squares equation that gives the relationship between the model parameters (**r**) and the data misfit (**g**) is given as follows:

$$[\mathbf{J}_i^T\mathbf{R}_d\mathbf{J}_i + \lambda_i\mathbf{W}^T\mathbf{R}_m\mathbf{W}]\ \Delta\mathbf{r}_i = \mathbf{J}_i^T\mathbf{R}_d\mathbf{g}_i - \lambda_i\mathbf{W}^T\mathbf{R}_m\mathbf{W}\mathbf{r}_{i-1}\ . \quad (1)$$

The Jacobian matrix **J** contains the sensitivities of the (logarithms of the) apparent resistivities with respect to the model resistivity values, **W** is the roughness filter (deGroot-Hedlin and Constable 1990), and λ is the damping factor. $\Delta\mathbf{r}_i$ is the required change in the model parameters (the logarithms of the model resistivity values) to reduce the data misfit **g**, while $\mathbf{r}_{i-1}$ is the resistivity model from the previous iteration. $\mathbf{R}_d$ and $\mathbf{R}_m$ are weighting matrices used by the L1-norm inversion method (Farquharson and Oldenburg, 1998; Loke *et al.* 2003) that was applied to both the data misfit and model roughness. The appropriate value of the damping factor λ can be estimated using the L-curve method (Farquharson and Oldenburg 2004; Loke, Dahlin and Rucker 2014). The inversion of a typical dataset usually takes five to eight iterations to converge.

SYNTHETIC MODELLING

We conducted tests using a synthetic model that simulates the geological environment in the field survey (Figure 2b). The model has two water layers of resistivity: 20 Ωm in the upper layer (12.25-m thick) and 10 Ωm that extends to the sea bottom. The sea bottom has a depth ranging from 7.0 m at the sides to 28.0 m in the middle. The bedrock has a resistivity of 2000 Ωm that is covered by a 3.6-m-thick layer of 100 Ωm that represents the overlying sediments. The pole–dipole array used in the field survey has 3256 data points and a maximum geometric factor of 16,628 m. The same pole–dipole array configurations were used for the synthetic model test. For the conventional array, we use all the possible "*a*" and "*n*" combinations for the Wenner–Schlumberger array for a survey line with 64 electrodes and 7.0-m spacing where the geometric factors were less than 16,628 m. This gave a dataset with 1963 data points. Voltage-dependent Gaussian random noise with an amplitude of 1 mΩ was added to the resistance values calculated with a finite-element forward modelling program for both arrays before they were converted into apparent resistivity values. This gave apparent resistivity datasets with average noise levels of 1.7% and 3.4%, respectively, for the Wenner–Schlumberger and pole–dipole arrays. Tests were also carried out with the dipole–dipole array, but the potentials calculated for the model (Figure 2a) for some array configurations were very low. In some cases, they were lower than the noise added, resulting in negative potentials.

The inversion of the Wenner–Schlumberger dataset converged to a data misfit of 1.7%, which is the same as the noise added. The Wenner–Schlumberger array inverse model displays a low-resistivity anomaly at vertical dike location to about 12 m below the sea bottom (Figure 2b). In contrast, the pole–dipole array inverse model shows the low-resistivity structure to about 60 m below. The data misfit of 3.5% is higher but is close to the noise level added. This shows that the pole–dipole array has a larger depth of investigation. This comes at the expense of placing the second current electrode at a sufficiently far distance from the survey line. The lower resistivity layer above the bedrock is not well resolved in both models. This is probably because most of the current flows through the water layer that has a much lower resistivity. This results in relatively poor resolution of the sub-bottom materials compared with a survey on land.

We also attempted an inversion of the dataset using a single water layer with an averaged resistivity of 15 Ωm (Figure 2d). As this is higher than the resistivity of the second layer, it causes a severe artefact in the form of a very-low-resistivity top layer below the water bottom. Furthermore, the resolution of the vertical zone is much poorer. This illustrates the importance of using the correct resistivity distribution in the water layer.

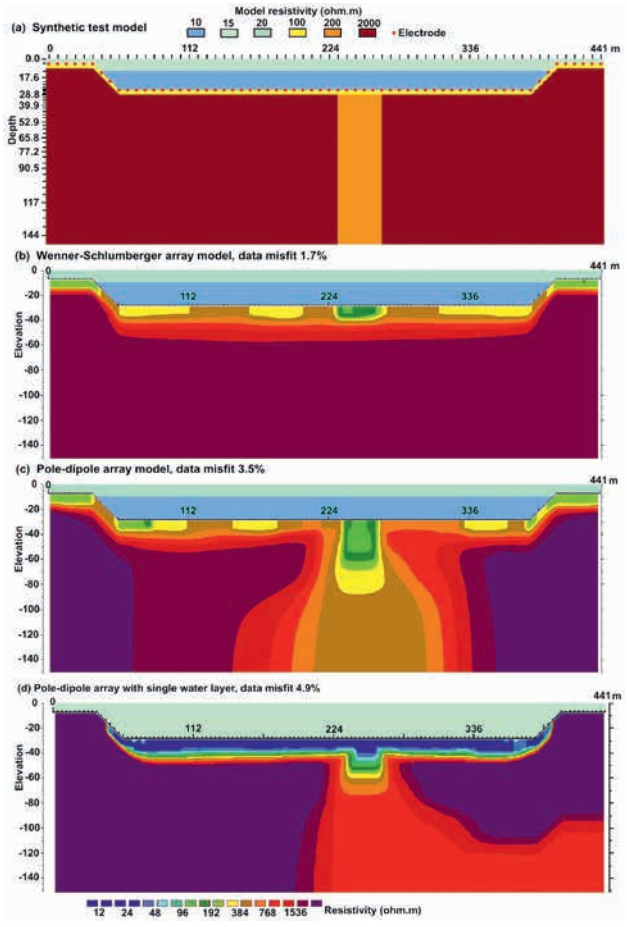

Figure 2 (a) Synthetic test model. Inverse models for the (b) Wenner–Schlumberger array, (c) pole–dipole array, and (d) pole–dipole array with incorrect single water layer.

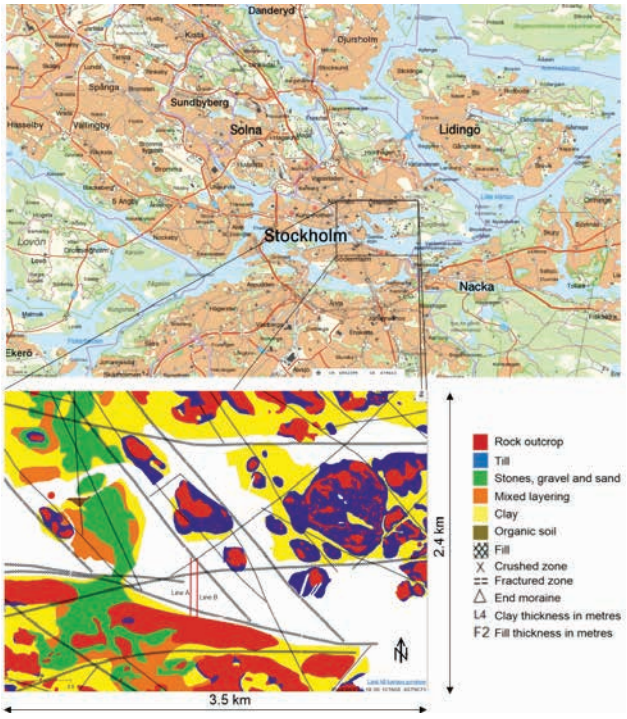

Figure 3 Location of test area in central Stockholm with detail from the engineering geological map of the field test area with the position of test lines marked with red (© Lantmäteriet; Stockholm Municipality 1997).

Figure 4 Deployment of electrode cable in progress.

FIELD SURVEY

Site description

An underwater ERT survey was carried out in a part of the sea called Saltsjön (Salt Lake) in downtown Stockholm (Figure 3), as part of pre-investigations for a new tunnel for a new line for the Stockholm metro (T-bana). The aim was to identify variations in the depth of the bottom sediments and variations in rock quality and the possible presence of weak zones in the rock. The bedrock on the islands surrounding the investigated area consists of granite, granodiorite, and metagreywacke with mica schist. Several tectonic zones with different directions are expected, and tectonic breccia and myolinite have been mapped nearby (Stockholm Municipality 1997; Persson 1998; Persson, Sträng and Antal 2001). The soil layers covering the bedrock are expected to include till and various recent sediments (Morfeldt 1993).

The site is rather difficult from a survey point of view. Seismic investigations nearby have not been successful due to gas in the bottom sediments. Electromagnetic methods were ruled out because of electric cables lying on the sea bottom. The variation in water depth, as well as vertical and lateral variation in salinity, requires attention. Furthermore, the rather intense boat traffic in the area puts demands and restrictions on survey logistics. An advantage is that the brackish water at the site is much less conductive than sea water in the oceans with a typical salinity around 3.5%.

Five ERT lines were measured using the same setup. Two of the lines were measured along the planned City Link high voltage power supply tunnel, which will be constructed near one of the alternative positions for the Nacka metro line tunnel. The intention was to use existing geotechnical drilling data for verification and calibration purposes.

ERT

The ERT surveys were performed using an electrode cable with 64 electrodes, which was placed on the seabed, Figure 4 shows deployment of the cable in progress. A truck was used to place a concrete block on the sea bottom, which was used as anchor to secure that the start position of electrode on cable was fixed when deploying it (Figure 5). The electrode take-out spacing was 7 m, giving a total layout of 441 m. Pole–dipole configuration was used in order to maximise depth penetration, where a 3500-m-long cable was used for the remote electrode that was placed in the water east of the study area. The remote electrode was placed almost perpendicular to the survey line, and thus, it was at almost the same distance from the potential electrodes for all the arrays used. As a consequence, the effect of the remote electrode on the measured apparent resistivity values is estimated to be less than 0.1% by comparing the geometric factors of the arrays used with and without the remote electrode included in the calculations.

The field survey was completed in three days, where one line was measured during the first day when time was also spent on installing the remote electrode apart from deploying the electrode cable, taking the ERT measurements, logging the water resistivity, recovering the electrode cable, etc.

A measurement protocol with 3256 data points per measurement line was used to provide good resolution and depth penetration. An ABEM Terrameter LS with 12 measurement channels was used for the measurements, where multi-channel measurement provided a quick measurement process despite the large number of data points. Interpreted sections of the resistivity distribution in the bottom sediments and bedrock were created using the inversion software Res2dinvx64. L1 norm (robust) inversion with water overlying the electrodes used (Loke *et al.* 2003; Loke and Lane 2004). The inversion software was adapted

to meet the requirements of this project by allowing several water layers with different resistivity.

Water depth and resistivity

In order to be able to get useful estimates of resistivity in soil and rock, it is necessary to integrate the water depth and the resistivity of the water in the interpretation model. Errors in water depth or resistivity lead to artefacts in the model, as the inversion program compensates for surplus or deficit in conductance in the water model by the corresponding increase or decrease in the resistivity. In this case, the bottom topography varies greatly, and the resistivity varies with depth in the sea; hence, it is of utmost importance to measure both bottom topography and resistivity depth distribution in the water for each survey line to avoid misleading results.

The water depth in the study area was mapped using multibeam sonar. The location of the survey lines was measured using side scan sonar where the measuring cable was identified in the measurement results. Depth profiles of the survey lines were then calculated by extracting information from the deep water model of the area along these lines (see Figure 6 for example). For quality assurance, the electrode cable was fitted with five automatically recording pressure transducers of type Diver that were used to calculate the depth in a number of reference points.

The water resistivity as a function of depth was measured with an ABEM Terrameter SAS4000 together with a SASLOG borehole log was used for measuring resistivity (see example in Figure 7).

RESULTS AND INTERPRETATION

The inspection of full waveform recordings done throughout the measurements reveals that there are high noise levels including 50 Hz and 16⅔ Hz and strong variation in background levels within the measurement cycles (see example in Figure 8). The 16⅔ Hz noise is most likely caused by train traffic, as it is the operating frequency of the Swedish rail system. The variation in background level may be caused by, for example, the underground train system (T-bana) that operates with DC power supply, or the variation in the load in the commuter and national rail systems.

Despite the noise, resistivity data are of sufficiently good quality so that no culling of data points was needed before further processing, as shown by the pseudosection plots that are shown separately for reverse and forward arrays for two out of six n-factors used (Figure 9). The bottom topography based on a combination of sonar surveying and pressure sensors was included as part of the models. The water resistivity distribution was approximated as a model of five layers with different resistivity. Each layer is assumed to be homogeneous in the horizontal direction; the variation in resistivity close to the surface was considered to be of limited importance.

The inversion resulted in models showing vertical sections of resistivity variation, and the results for Line A, which is one of the lines with drilling reference data, are shown in . The models have acceptable residuals (about 6%–7%), which show that there is relatively good agreement between model and data. The resistivity sections show fluctuations that can be interpreted as a superficial layer with lower resistivity, which probably can be associated with soil layers of varying thickness and composition. Below, there are generally higher but varying resistivities that can be interpreted as bedrock zones of weakness and possibly varying composition. The top of the inverted sections is characterised by resistivities substantially lower than 12 Ωm with maximum thicknesses of up to about 20 m in the central parts of the lines. This can be interpreted as unconsolidated sediments.

In the distance range of 220–440 m on Line A (Figure 10), there is a zone with resistivities in the range of 12–36 Ωm in the upper low-resistivity zone down to several tens of metres. A corresponding zone appears on the other nearby lines, which could have been interpreted as a zone of anomalous composition of the rock or fractured and weathered rock. Alternatively, it could be interpreted as a sharp increase in depth to bedrock, where the

Figure 5 Measurement in progress with the ferry passing over the survey line. The survey boat used for deployment of the electrode cable, sonar depth mapping, etc., is visible in the foreground. The truck was used to place a concrete block on the sea bottom, which was used as anchor to secure that the start position of electrode on cable was fixed when deploying it.

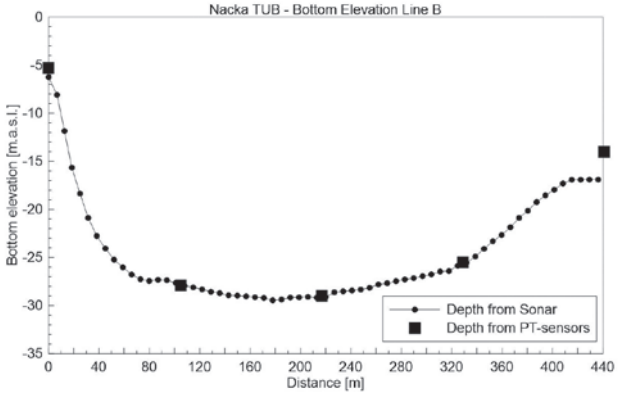

Figure 6 Example of depth profile determined with sonar and pressure sensors.

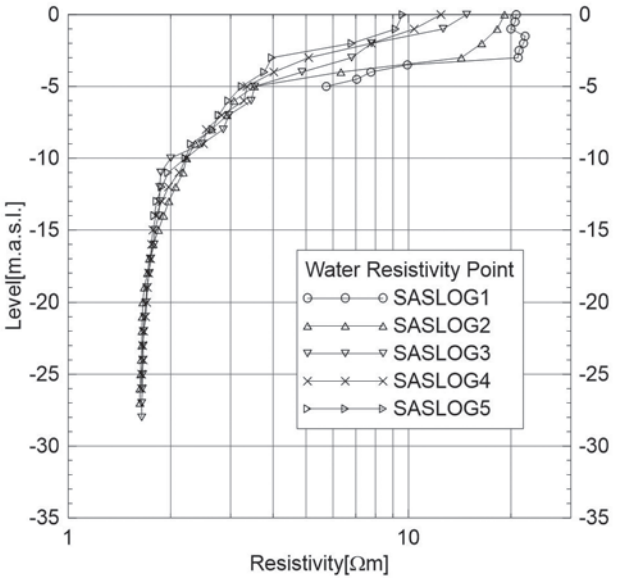

Figure 7 Water resistivity variation as a function of depth.

rock is overlain by sediments with different composition or salinity compared with the upper parts of the sediments. At the beginning of each line, low resistivities indicate that there may be a zone of weakness in the rock, which is expected from the engineering geological map (Figure 3). Since the zone is located at the edge of the lines, the resolution is, however, poor. The low resistivity at the edge might also be caused by structural elements in quay construction, but because the survey lines are oriented perpendicular to the layout direction, impact should be relatively limited.

There are more or less vertical structures in the deeper parts of the sections that can be interpreted as tectonic zones and separating more highly resistive zones (>1000 Ωm) from zones with intermediate resistivities (a few hundred Ωm). The high-resistivity zones can be interpreted as crystalline rock with low degree of fracturing, whereas the zones of lower resistivity can be interpreted as rock with differing quality that is probably fractured and weathered rock.

Interpreted depths to bedrock from geotechnical drilling have been superimposed in the resistivity section of Line A (Figure 10). Interpreted depth to rock is generally well consistent between methods. Local deviations, apart from resolution limitations, in the depths may be due, for example, to the rock surface topography varying in three dimensions, whereas the ERT survey is based on a 2D approximation of reality. Rock levels show that the zone of relatively low resistivity in the range 220–440 m on line A consists of low-resistivity rock, which may be the uppermost part of a larger zone of differing properties of the rock. The successful determination of the bedrock level, much better than indicated by the synthetic example, is probably due to that the bottom sediment resistivities are in the same order as the resistivity of the brackish water in addition to the substantial thickness.

CONCLUSIONS

An approach for integrating and accounting for water layers with different resistivity has been demonstrated to work. Synthetic modelling shows thin layers and a sub-bottom sediment layer with exaggerated thickness. In the presented example, pole–dipole array data hold a clear advantage over Wenner–Schlumberger data in terms of resolution of a vertical zone of intermediate resistivity, which is intended to represent a fractured bedrock zone. The synthetic modelling also clearly shows that severe artefacts can arise from using a simplified approach with averaged water resistivity instead of the actual resistivity layering in the inversion.

The field example results show that the rather difficult survey conditions could be handled in a satisfactory way thanks to adequate equipment, careful planning, and attention to details. The resistivity of the brackish water limits the resolution capability of the methods due to short circuiting in the water layer, but on the other hand, the conditions are much more favourable than in the oceans with their higher-salinity water.

The measured data contain information that is relevant for creating coherent models of the variation in depth to rock that are

i n

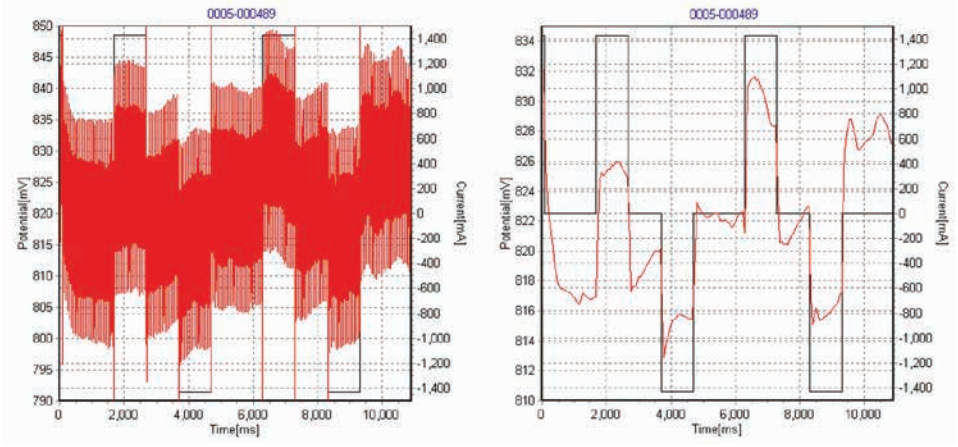

Figure 8 Example of full waveform recording (a) raw data, (b) averaged over 60-ms multiples.

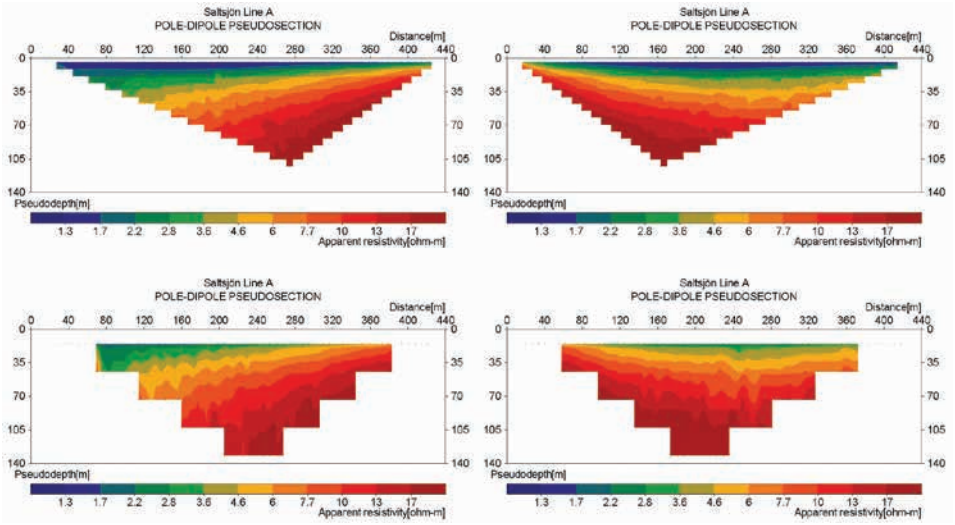

Figure 9 Example subsets of measured data for Line A in Saltsjön plotted as pseudosections ($n = -1$, $n = 1$, $n = -5$, and $n = 5$).

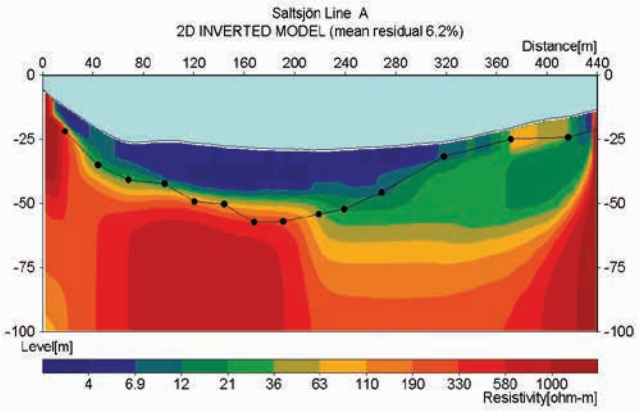

Figure 10 Resistivity model for Line A in Saltsjön, with water levels and interpreted depth to the bedrock from the geotechnical drilling indicated (vertical exaggeration factor 2).

good agreement with depth to bedrock data from geotechnical drilling. The results also indicate that information on variation in rock quality that can be of critical importance for planning of underground construction can be derived from the data. Additional reference data would be required for a full evaluation of the results.

ACKNOWLEDGEMENTS

The authors thank Stockholms Läns Landsting (SLL) who financed the T-bana Nacka survey for permission to publish the results. We also wish to thank Roberth Colliander at WSP and Thomas Sträng at SSL for their good cooperation throughout the project. Funding that made this work possible was provided by BeFo, Swedish Rock Engineering Research Foundation (ref. 331); SBUF, The Development Fund of the Swedish Construction Industry (ref. 12719); and Formas, The Swedish Research Council for Environment, Agricultural Sciences and Spatial Planning, for the presentation of the results (ref. 2012-1931) as part of the Geoinfra-TRUST framework (http://www.trust-geoinfra.se/).

REFERENCES

Dahlin T., Bjelm L. and Svensson C. 1999. Use of electrical imaging in the site investigations for a railway tunnel through the Hallandsås Horst, Sweden. *Quarterly Journal of Engineering Geology and Hydrogeology* **32**, 163–173

Danielsen B.E. and Dahlin T. 2009. Comparison of geoelectrical imaging and tunnel documentation. *Engineering Geology* **107**(3–4), 118–129.

deGroot-Hedlin C. and Constable S. 1990. Occam's inversion to generate smooth, two-dimensional models form magnetotelluric data. *Geophysics* **55**(12), 1613–1624.

Dey A. and Morrison H.F. 1979. Resistivity modelling for arbitrary shaped two-dimensional structures. *Geophysical Prospecting* **27**(1), 106–136.

Farquharson C.G. and Oldenburg D.W. 1998. Nonlinear inversion using general measures of data misfit and model structure. *Geophysical Journal International* **134**(1), 213–227.

Farquharson C.G. and Oldenburg D.W. 2004. A comparison of automatic techniques for estimating the regularization parameter in non-linear inverse problems. *Geophysical Journal International* **156**(3), 411–425.

Ganerød G.V., Rønning J.S., Dalsegg E., Elvebakk H., Holmøy K., Nilsen B. *et al*. 2006. Comparison of geophysical methods for subsurface mapping of faults and fracture zones in a section of the Viggja road tunnel, Norway. *Bulletin of Engineering Geology and the Environment* **65**, 231–243.

Lile O.B, Backe K.R., Elvebackk H. and Buan J.E. 1994. Resistivity measurements on the sea bottom to map fracture zones in the bedrock underneath sediments, *Geophysical Prospecting* **42**(7), 813–824.

Loke M.H., Acworth I. and Dahlin T. 2003. A comparison of smooth and blocky inversion methods in 2D electrical imaging surveys. *Exploration Geophysics* **34**(3), 182–187.

Loke M.H. and Barker R.D. 1996. Rapid least-squares inversion of apparent resistivity pseudosections using a quasi-Newton method. *Geophysical Prospecting* **44**(1), 131–152.

Loke M.H., Dahlin T. and Rucker D.F. 2014. Smoothness-constrained time-lapse inversion of data from 3D resistivity surveys. *Near Surface Geophysics* **12**, 5–24.

Loke M.H. and Lane J.W. 2004. Inversion of data from electrical resistivity imaging surveys in water-covered areas. *Exploration Geophysics* **35**(4), 266–271.

Morfeldt C.O. 1993. Underground construction on engineering geological terms: a fundamental necessity for the function of metropolitan environments and man's survival. *Engineering Geology* **35**(3–4), 149–165.

Nyquist J.E., Freyer P.A. and Toran L. 2008. Stream bottom resistivity tomography to map ground water discharge, *Ground Water* **46**(4), 561–569.

Nyquist J.E., Heaney M.J. and Toran L. 2009. Characterizing lakebed seepage and geologic heterogeneity using resistivity imaging and temperature measurements. *Near Surface Geophysics* **7**(5-6), 487 – 498.

Orlando L. 2013. Some considerations on electrical resistivity imaging for characterization of waterbed sediments. *Journal of Applied Geophysics* **95**, 77–89.

Persson L. 1998. Engineering geology of Stockholm, Sweden. *Bulletin of Engineering Geology and the Environment* **57**(1), 79–90.

Persson L., Sträng M. and Antal I. 2001. *Berggrundskartan 10I Stockholm (Bedrock Map 101 Stockholm*), Scale 1:100 000, Series Ba, No. 60, Swedish Geological Survey, Uppsala.

Ronczka M., Hellman K., Günther T., Wisen R. and Dahlin T. 2017. Electric resistivity and seismic refraction tomography: a challenging joint underwater survey at Äspö Hard Rock Laboratory. *Solid Earth*, **8**(3), 671–682.

Rønning J.S., Ganerød G., Dalsegg E. and Reiser F. 2013. Resistivity mapping as a tool for identification and characterisation of weakness zones in crystalline bedrock: definition and testing of an interpretational model. *Bulletin of Engineering Geology and the Environment*, **73**(4), 1225–1244.

Silvester P.P. and Ferrari R.L. 1990. *Finite Elements for Electrical Engineers*,2nd ed. Cambridge University Press.

Simyrdanis K., Papadopoulos N., Kim J.-H., Tsourlos P. and Moffat I. 2015a. Archaeological investigations in the shallow seawater environment with electrical resistivity tomography. *Near Surface Geophysics* **13**(6), 601–611.

Simyrdanis K., Tsourlos P., Soupios P., Tsokas G., Kim J.-H. and Papadopoulos N. 2015b. Surface-to-tunnel electrical resistance tomography measurements. *Near Surface Geophysics* **13**(4), 343–354.

Stockholm Municipality 1997. *Byggnadsgeologisk karta (Engineering Geological Map)*, https://iservice.stockholm.se/open/GeoArchive/Pages/Search.aspx (accessed 2014-04-15).

Tassis G.A., Tsourlos P.I., Rønning J.S. and Dahlin T. 2014. Detection and characterization of fracture zones in bedrock: possibilities and limitations. *Proceedings of Near Surface Geoscience 2014*, Athens, Greece, September 2014, 5p. EAGE.

Tsourlos P. and Tsokas G.N. 2004. Underwater resistivity surveying for sludge layer parametrization. *Proceedings of the 1st International Conference on Advances in Mineral Resources Management and Environmental Geotechnology, AMIREG 2004*, Crete, Greece, June 2004, pp. 113–118. Heliotopos Conferences.